Crystallization of Isotactic Polypropylene under High Pressure (γ Phase)

C. Angelloz, R. Fulchiron,* A. Douillard, and B. Chabert

Laboratoire des Matériaux Polymères et des Biomatériaux, UMR-CNRS 5627, Université Claude Bernard, ISTIL, 43 bd du 11 Novembre 1918, 69622 Villeurbanne Cedex, France

R. Fillit and A. Vautrin

Centre Matériaux et Structures, Ecole Nationale Supérieure des Mines de Saint-Etienne, 158 cours Fauriel, 42000 Saint Etienne, France

L. David

Groupe d'Etudes de Métallurgie Physique et de Physique des Matériaux, UMR−CNRS 5510, Institut National des Sciences Appliquées de Lyon, bât. 502, 20 av Albert Einstein, 69621 Villeurbanne Cedex, France

Received October 28, 1999; Revised Manuscript Received March 23, 2000

ABSTRACT: Isothermal crystallization of isotactic polypropylene at high pressures (from 200 to 250 MPa) have been carried out using a high-pressure dilatometer leading to a pure γ-form, as revealed by WAXD. The melting temperatures at the same pressures have been determined to assess the pressure effect on the equilibrium melting temperature by the Hoffman−Weeks analysis. The crystallization times have been analyzed according to the Hoffman−Lauritzen theory and corrections introduced to take into account the pressure effects on both the equilibrium melting temperature and the diffusion process. This analysis showed a transition from crystallization regime II to regime III for an undercooling of 53.7 K. The lateral and fold surface free energies were evaluated. Furthermore, the morphology of the samples investigated by polarized light microscopy, density measurements, and SAXS depends only on the crystallization undercooling, as a result of the influence of pressure on the equilibrium melting temperature. Moreover, the lamellar thickness experimental data agree well with the theoretical calculation.

Introduction

Isotactic polypropylene (iPP) can crystallize in several forms denoted α, β, and γ. The monoclinic α phase[1,2] was first established by Natta and Corradini. The pseudohexagonal β structure, despite its discovery many years ago,[3] has been elucidated only recently.[4,5] Among these crystalline structures, the γ form is certainly the most peculiar considering the nonparallel chain axes, coexisting in the orthorhombic unit cell which was first proposed by Brückner and Meille.[6,7] Along the *c*-axis of the cell, 4 bilayers of helices range with a tilt of 81° from one to the other (at ±40° to the lamellar normal). This peculiar structure, unique for polymers, is now well established.[8,9] At atmospheric pressure, the γ phase appears under various conditions, for instance when the polymer chains are short[10] or in the case of a copolymer ethylene-propylene with a small amount of ethylene.[11,12] However, the main way to obtain γ structure for a high molecular weight homopolymer is to perform crystallization under high pressure;[7,13] this structure becoming dominant at pressures higher than 200 MPa.[14,15]

There are several morphological analyses of the γ phase of iPP obtained under high pressure described in the literature. Mezghani and Phillips reported important works concerning the phase diagram of iPP and the equilibrium melting point of the γ phase.[16−18] Among different techniques, they used a high-pressure cell mounted on a microscope under cross-polar conditions allowing them to observe the spherulites growth and to measure the pressure dependence of the melting point up to 200 MPa. Particularly, they showed that the birefringence of the pure γ-form spherulites can be positive or negative depending on the crystallization undercooling[17] in relation to the crystallization regime.[19]

Besides, the crystallization kinetics under high pressure can be studied by dilatometry but experimental data for iPP are limited[20,21] and not specifically dedicated to the γ phase. In the present work, the dilatometry is used to analyze the crystallization of iPP for pressures higher than 200 MPa in order to ensure the dominance of the γ structure and thus to avoid a mixing of α and γ phases. The crystallization kinetics is discussed on the basis of the Lauritzen−Hoffman equation, and the resulting morphology is studied.

Theoretical Background

Crystallization Kinetics. The surface nucleation theory of Lauritzen and Hoffman[22,23] is widely used to describe the crystallization growth from the melt. Recently, Hoffman and Miller[24] published a very comprehensive paper revisiting the theory and incorporating new developments. The spherulite or axialite linear growth rate for a temperature T can be expressed by the well-known equation

$$G = G_0 \exp\left[\frac{-U^*}{R(T - T_\infty)}\right]\exp\left[\frac{-K_g}{T(\Delta T)f}\right] \qquad (1)$$

where the preexponential factor G_0 is almost indepen-

* To whom correspondence should be addressed. E-mail: fulchiro@matplast.univ-lyon1.fr.

10.1021/ma991813e CCC: $19.00
Published on Web 05/04/2000

dent of the temperature. The first exponential term of eq 1 accounts for the chain motion in the melt[25] where R is the gas constant, T_∞ is a temperature often close to $T_g - 30$ K, and U^* is an energy parameter similar to an apparent activation energy of motion. In this paper, the used value of T_∞ is 233 K[26] and U^* is assumed to be close to 6280 J/mol since this value is generally applied to polypropylene.[23,27−29] This mobility factor can also be replaced by an alternative expression such as $\exp[-Q^*_D/RT]$ where Q^*_D is the activation energy for the diffusion mechanisms such as reptation.[30] Other theories invoking the concept of cooperativity can also be used, leading to a different mobility factor.[31,32] The second exponential term contains the secondary nucleation effect on the growth front. In this term, $\Delta T = T_m^0 - T$ is the undercooling, where T_m^0 is the equilibrium melting temperature; $f = 2T/(T_m^0 + T)$ is a correction factor used for the variation of the heat of fusion with the temperature. The parameter K_g can be expressed as

$$K_g = \left[\frac{jb_0\sigma\sigma_e T_m^0}{k(\Delta h_f)}\right] \tag{2}$$

where $j = 2$ for regime II and $j = 4$ for regimes I and III, b_0 is the crystalline layer thickness, Δh_f is the heat of fusion per unit volume, σ_e is the fold surface free energy, σ is the lateral surface free energy, and k is the Boltzmann constant. Knowing the growth rate G, one obtains the value of K_g from a plot of $\ln G + U^*/R(T - T_\infty)$ vs $1/fT(\Delta T)$.

Lamellar Thickness. From the surface nucleation model, the initial lamellar thickness can be obtained[22,24]

$$l_g^* = \frac{2\sigma_e T_m^0}{\Delta h_f \Delta T} + \delta \tag{3}$$

where δ is given by

$$\delta = \frac{kT}{2b_0\sigma}\left[\frac{a_0\Delta h_f\Delta T + 4\sigma T_m^0}{a_0\Delta h_f\Delta T + 2\sigma T_m^0}\right] \tag{4}$$

a_0 is the width of the tertiary crystalline germ likened to the molecule width.

In eq 4, the lateral surface free energy σ must be determined by another way than eq 2 which provides only the product $\sigma\sigma_e$. Hoffman[33] suggested a relationship between the lateral surface free energy and the characteristic ratio of the polymer chain C_∞[34]

$$\sigma = \frac{a_0\Delta h_f l_b}{2l_u C_\infty} \tag{5}$$

where l_b is the C−C bond length and l_u is the C−C distance as projected along the chain axis.

Thus, combining eq 2 with eq 5, an expression of σ_e is obtained:

$$\sigma_e = \frac{2kK_g C_\infty l_u}{ja_0 b_0 T_m^0 l_b} \tag{6}$$

Experimental Section

Material. The studied isotactic polypropylene was supplied by the company Atochem. This homopolymer was obtained using the Ziegler−Natta catalysts process. The molecular weight characteristics of this material were: $M_w = 234\,000$ g/mol, $I_p = 5.2$ (measured by Atochem) with an isotactic dyads content of 93.1% determined using ^{1}H NMR.

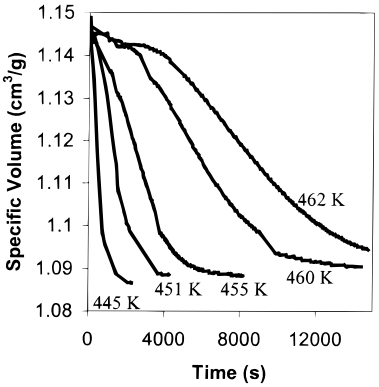

Figure 1. Typical variations of the specific volume for various crystallization temperatures ($P = 200$ MPa).

Dilatometry Measurements. The main part of the experiments on crystallization kinetics was performed using a high-pressure dilatometer PVT100 from SWO Polymertechnik GmbH which yields the variation of the length of the sample (about 15 mm) between a fixed and a mobile pistons in a pressure cell of 7.7 mm of diameter. The weight of the sample is about 0.6−0.7 g. The length is then converted into specific volume. This setup can operate between 15 and 250 MPa.

Isothermal crystallization experiments were carried out using the following procedure: the polymer sample was heated to 483 K under atmospheric pressure during five minutes. Then, it was cooled to the desired crystallization temperature T (in the range from 443 to 467 K). Afterward, the desired pressure P was applied. This procedure allowed to reach the suitable temperature and pressure conditions before the beginning of the crystallization since the raise of the pressure is fast. Typical curves of specific volumes are shown in Figure 1. From the evolution of the specific volume vs time, the relative crystallinity $\alpha(t)$ is obtained according to

$$\alpha(t) = \frac{X_m(t)}{(X_m)_\infty} = \frac{V_0 - V(t)}{V_0 - V_\infty} \tag{7}$$

where $X_m(t)$ is the mass crystallinity at the time t, $(X_m)_\infty$ is the mass crystallinity at the end of the experiment, and V_0, $V(t)$, and V_∞ are the specific volumes at $t = 0$, at time t and at the end of the experiment, respectively.

After each isothermal crystallization, the sample was cooled to room temperature without releasing the pressure. Then, the melting temperature of the sample was measured under the same pressure using an isobaric heating at 5 K/min. The corresponding melting temperature T_m was then chosen at the halfway point of the melting transition as shown in Figure 2.

Polarized Light Microscopy. The spherulites were observed by Polarized light microscopy with a Leitz Orthoplan microscope in microtomed sections of samples crystallized at high pressure in the dilatometer.

X-ray Structural Characterization. The morphology of the high-pressure crystallized samples was studied by wide-angle X-ray diffraction (WAXD) and small-angle X-ray scattering (SAXS) using Cu Kα radiation.

Wide-angle X-ray diffraction experiments were carried out on the high pressure isothermally crystallized samples (ranging between 200 and 250 MPa) and compared with a low-pressure crystallized sample (15 MPa). The diffraction patterns, after subtraction of the amorphous component are shown in Figure 3 where the indexing have been carried out from the α-iPP[2,35] and γ-iPP[6,35] cell parameters. For crystallization pressure greater than 200 MPa, the (130) peak characteristic of the α phase at the scattering angle 2θ of 18.6°

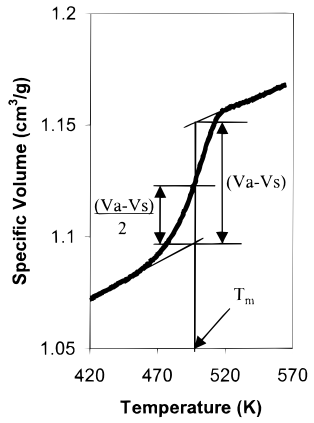

Figure 2. Typical specific volume curve during isobaric melting experiment (P = 200 MPa, heating rate 5 K/min, previous crystallization temperature = 445 K).

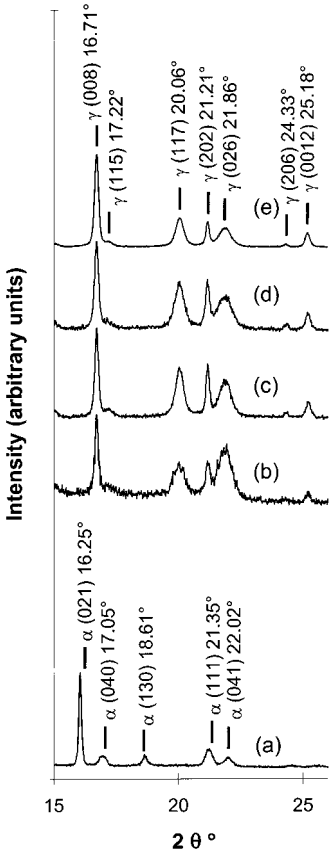

Figure 3. X-ray diffraction profiles for various crystallization conditions: (a) $T = 414$ K, $P = 15$ MPa; (b) $T = 445$ K, $P = 200$ MPa; (c) $T = 458$ K, $P = 200$ MPa; (d) $T = 453$ K, $P = 250$ MPa; (e) $T = 192$ K, $P = 250$ MPa.

does not appear anymore whereas the (117) peak characteristic of the γ phase at the scattering angle 2θ of 20.1° is detected. Thus, it is concluded that, in these crystallization pressure and temperature ranges, the γ phase is formed exclusively.

Small-angle X-ray scattering experiments were performed in order to obtain the long period (L) in the iPP samples crystallized under high pressure. The SAXS device included a rotating anode a point collimation system consisting in two crossed total reflection mirrors and a line-position-sensitive proportional counter as decribed elsewhere.[36]

Two methods were used to deduce L. First, the position q_{max} of the maximum of the Lorentz-corrected intensity $I_1(q) = q^2I(q)$ was calculated by a local parabolic least-squares fit. As usual, q is the scattering vector and $I(q)$ is the background-corrected scattered intensity. The Bragg's law is then applied

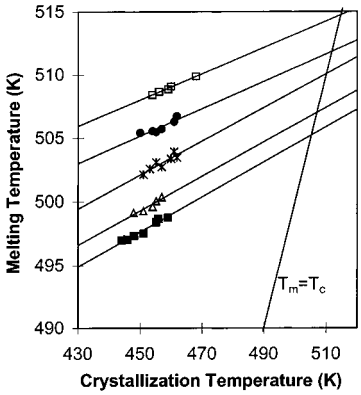

Figure 4. Hoffman−Weeks plots for different pressures: (□) 250 MPa; (●) 238 MPa; (∗) 225 MPa; (△) 212 MPa; (■) 200 MPa.

to deduce L from the relation

$$L = \frac{2\pi}{q_{max}} = \frac{\lambda}{2\sin(\theta_{max})} \tag{8}$$

where λ is the incident wavelength and $2\theta_{max}$ is the scattering angle at the maximum of I_1.

The second method used consisted in the calculation of the monodimensional correlation function $\gamma(r)$, defined as

$$\gamma(r) = \frac{\int_0^\infty q^2 I(q)\cos(qr)\,dq}{\int_0^\infty q^2 I(q)\,dq} \tag{9}$$

To calculate the integrals defined above, an extrapolation of the data for the small q and for the large q ranges was necessary. A linear dependence of $I(q)$ with q was chosen at low q, and the Porod's asymptote ($I(q) = C/q^4$) was used for the large q range. The Porod's constant C was determined by a least-squares fit of the large q tail of the scattered intensity. The first maximum of the correlation function $\gamma(r)$ finally yields the long period.

In all cases, the values deduced by both methods were in very good agreement (within 2 or 3 Å). Detailed reviews of the different possible methods that can be used for the determination of the long period can be found in the literature, including the effects of the variances of the distributions of amorphous and crystalline thickness.[37]

Crystallinity Determination. The density of the samples was measured by a classical gradient column method using ethanol and water mixtures. The crystallinity was then derived from the densities of the crystalline γ phase and the amorphous phase using

$$X_m = \frac{\rho_c}{\rho}\frac{\rho - \rho_a}{\rho_c - \rho_a} \tag{10a}$$

$$X_v = \frac{\rho - \rho_a}{\rho_c - \rho_a} \tag{10b}$$

where X_m is the mass crystallinity, X_v is the volume crystallinity, ρ is the sample density, ρ_c is the γ crystalline phase density[38] ($\rho_c = 0.938$ g·cm^{-3}), and ρ_a is the amorphous phase density[39] ($\rho_a = 0.854$ g·cm^{-3}).

Results and Discussion

Crystallization Kinetics. First, the effect of the pressure on the equilibrium melting temperature was analyzed by means of Hoffman−Weeks plots[40] for different pressures of crystallization and melting. The results are summarized in Figure 4. The linear pressure dependence of the equilibrium melting temperature is

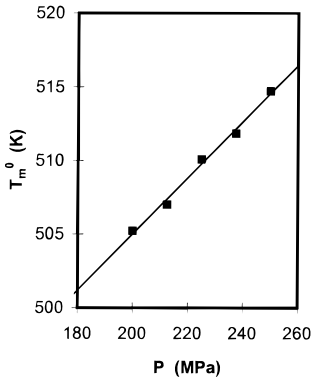

Figure 5. Equilibrium melting temperature of γ phase as a function of pressure.

plotted in Figure 5. The linear regression on the measured values leads to

$$T_m^0\,(\mathrm{K}) = 466.9 + 0.191P\,(\mathrm{MPa}) \qquad (11)$$

This last equation is comparable to the results of Mezghani and Phillips,[16,18] who studied the melting behavior of iPP by means of a depolarized light intensity method under pressure up to 200 MPa. For this pressure, they reported an equilibrium melting temperature of 514 K while eq 11 leads to 505 K. The difference can be explained by the different levels of microstructural impurities[19] or by the measurement method itself. Indeed, in the present work, the melting temperature T_m was chosen at the half of the melting transition (see Figure 2) whereas their values rather corresponds to the end of the melting.

The crystallization kinetics was then analyzed from the specific volume curves obtained at constant temperature and pressure, by means of the half-crystallization time values ($t_{1/2}$). Indeed, from an overall kinetics of Avrami approach,[41] in the case of instantaneous nucleation as generally accepted for iPP, the Avrami exponent is close to 3 and the transformed fraction is written as

$$\alpha(t) = 1 - \exp\left(-\frac{4\pi N G^3}{3} t^3\right) \qquad (12)$$

where N is the nuclei number.

Thus, the half-crystallization time can be expressed as

$$t_{1/2} = \left(\frac{3\ln(2)}{4\pi N}\right)^{1/3} G^{-1} \qquad (13)$$

Combining this last equation with eq 1, one obtains

$$(t_{1/2})^{-1} = G_0\left(\frac{4\pi N}{3\ln(2)}\right)^{1/3} \exp\left[\frac{-U^*}{R(T - T_\infty)}\right]\exp\left[\frac{-K_g}{T(\Delta T)f}\right] \qquad (14)$$

Nevertheless, in eq 12, the number of nuclei per unit volume N is temperature dependent. This was taken into account by measuring the average diameter of the spherulites from the polarized light micrographs of the samples crystallized at different conditions of temperature and pressure. Some of these micrographs are shown in Figure 6. Besides, the assumed value of 3 for the Avrami exponent in eq 12 is corroborated by the observed rectilinear boundaries between the spherulites.[42] Figure 7 shows the evolution of the number of nuclei vs the crystallization undercooling for our experimental bounding pressures, namely 200 and 250 MPa. As shown in this figure, the evolution of the number of nuclei can be empirically described by the

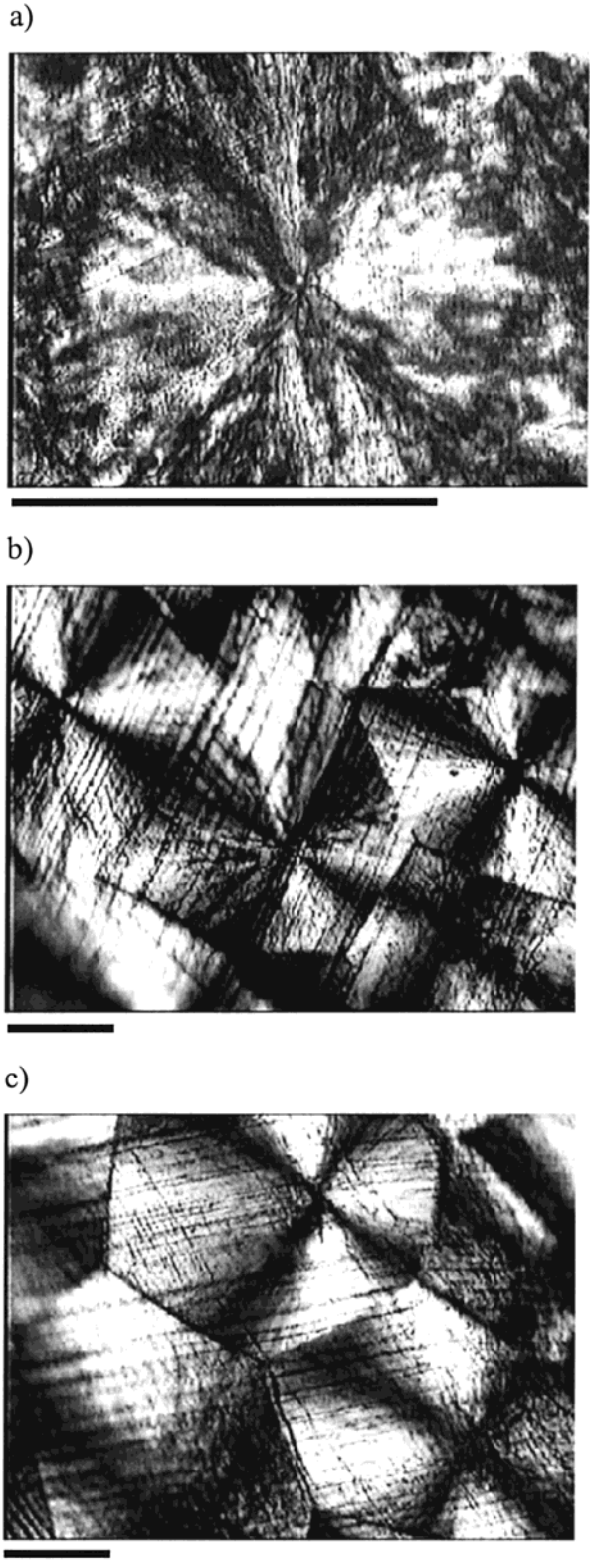

Figure 6. Polarized light micrographs of spherulites obtained from different conditions (scale bars: 100 μm): (a) 448 K, 200 MPa, $\Delta T = 56.9$ K; (b) 458 K, 250 MPa, $\Delta T = 56.4$ K; (c) 466 K, 250 MPa, $\Delta T = 48.5$ K.

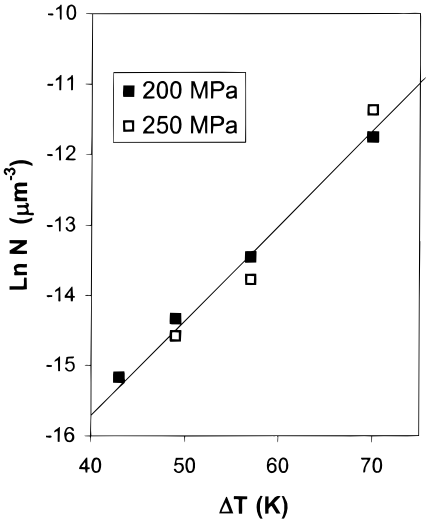

Figure 7. Evolution of the number of nuclei per unit volume vs the undercooling: (■) crystallization pressure 200 MPa; (□) crystallization pressure 250 MPa; (−) eq 15.

following equation

$$N = C \exp[\nu \Delta T] \tag{15}$$

with $C = 6.47 \times 10^{-10}\ \mu\text{m}^{-3}$ and $\nu = 0.1349\ \text{K}^{-1}$

It is not the purpose of this paper to discuss this evolution theoretically. However, an exponential variation of the number of heterogeneous nuclei with the temperature for polypropylene was already mentioned in the literature[43−45] at atmospheric pressure. In this work, the effect of the pressure is introduced considering its effect on the equilibrium melting temperature (eq 11) leading to the nuclei number only depending on the undercooling. Then, eq 14 can be rewritten

$$(t_{1/2})^{-1} = A \exp\left[\frac{\nu \Delta T}{3}\right] \exp\left[\frac{-K_g}{T(\Delta T)f}\right] \exp\left[\frac{-U^*}{R(T - T_\infty)}\right] \tag{16}$$

where A is temperature independent.

Moreover, since the equilibrium melting temperature is pressure dependent, the value of K_g is pressure dependent as well (see eq 2). The Hoffman−Lauritzen diagrams were thus obtained by plotting $-\ln t_{1/2} + U^*/R(T - T_\infty) - \nu\Delta T/3$ vs $T_m^0/fT(\Delta T)$ instead of $1/fT(\Delta T)$ as is the case for classical analysis of experiments at constant pressure. This diagram is shown in Figure 8 for the different pressures exhibiting both growth regimes II and III. In this Figure, the slopes are equal to $-K_g/T_m^0$, and they appear practically pressure independent as expected. The mean slope for regime III is 563 K and the mean slope for regime II is 289 K, leading-to-a ratio of 1.95 for a theoretical value of 2.

However, in Figure 8 the Hoffman−Lauritzen plot does not fall on a single curve meaning that additional parameters of the crystallization kinetics are pressure dependent. As a matter of fact, the effects of the pressure on the diffusion factor of eq 16 must be estimated.

This estimation can be achieved using results of viscosity measurements under pressure since the zero shear viscosity of melt polymers is governed by diffusion processes.[46] On the basis of zero shear viscosity measurements of numerous liquid and especially polymers, Cogswell and McGowan[47] could establish the following

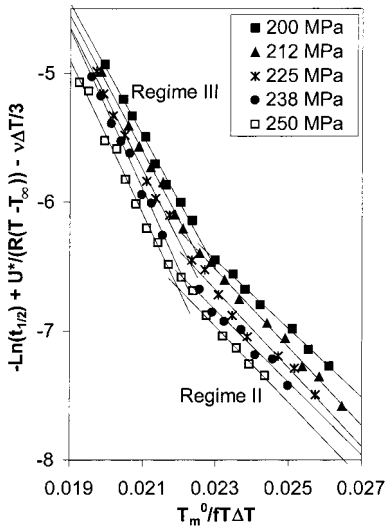

Figure 8. Hoffman−Lauritzen diagram for different pressures.

expression between viscosity, temperature, and pressure

$$\ln\left(\frac{\eta}{\eta^*}\right) = \frac{\ln(10)P^*V^*}{69RT}\left(32.25 - 32.25\frac{T}{T^*}\right)^{1/2} \times \left[9\frac{P}{P^*} + \left(32.25 - 32.25\frac{T}{T^*}\right)^{9/5}\right]^{5/9} \tag{17}$$

where P^* is 8.58×10^6 Pa for all liquids, T^* is a temperature characteristic of each liquid, and V^* is the size of the diffusing segment of polymer chain. Moreover, for entangled polymers the value of η^* is strongly molecular weight dependent since it varies as $M_w^{3.4}$. Nevertheless, in this work, only the reduced viscosity values η/η^* will be needed. In the case of polypropylene, using measurements in a temperature range of 463−503 K and a pressure range of 0.1−175 MPa the authors reported the following values: $T^* = 780$ K and $V^* = 0.001\ \text{m}^3\cdot\text{mol}^{-1}$.

The viscosity law of Cogswell and McGowan was fitted by means of a least squares minimization procedure, to a new expression for the mobility term of eq 16, where pressure effects are introduced according to

$$\ln\left(\frac{\eta}{\eta^*}\right) = \frac{U^* + \alpha P}{R(T - T_\infty)} + \beta P \tag{18}$$

where $\alpha = 3.88 \times 10^{-5}\ \text{J}\cdot\text{mol}^{-1}\cdot\text{Pa}^{-1}$ and $\beta = -4.35 \times 10^{-9}\ \text{Pa}^{-1}$.

The agreement between eq 17 and eq 18 is shown in Figure 9. It should be noticed that Kadijk and Van Den Brule[49] used an expression similar to eq 18 to describe the temperature and pressure variations of the zero-shear viscosity for different polymers including polypropylene. Moreover, the introduction in eq 18 of more pressure parameters, accounting, for example, for the variation of T_∞ with the pressure, does not yield to a better agreement with eq 17.

Equation 14 is rewritten as follows:

$$(t_{1/2})^{-1} = A \exp\left[\frac{\nu \Delta T}{3}\right] \exp\left[\frac{-K_g}{T(\Delta T)f}\right] \times \exp\left[-\frac{U^* + \alpha P}{R(T - T_\infty)} - \beta P\right] \tag{19}$$

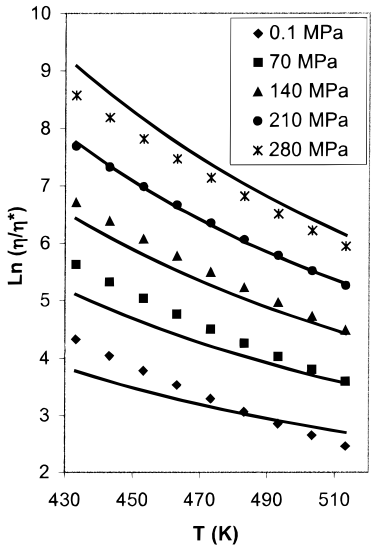

Figure 9. $\ln(\eta/\eta^*)$ vs T for various pressures: Symbols given by eq 17; full lines given by eq 18.

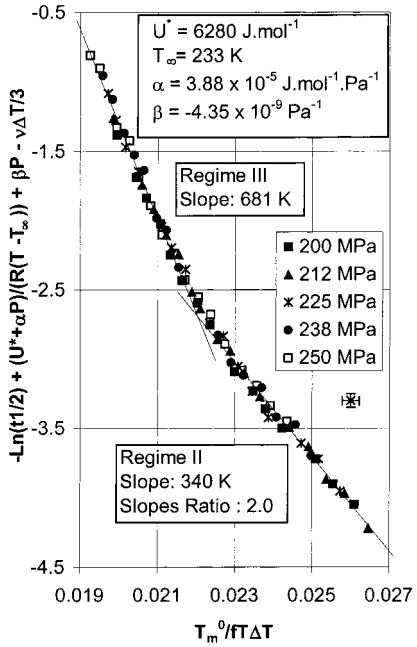

Figure 10. Modified Hoffman−Lauritzen diagram taking into account the effect of pressure on the diffusion term. (Error bars located below the legend are obtained considering an accuracy of ±5% for the half-crystallization times and ±0.5 °C for the crystallization temperature.)

Hence, from eq 19, a modified Hoffman−Lauritzen diagram has been constituted by plotting $-\ln t_{1/2} + (U^* + \alpha P)/R(T - T_\infty) + \beta P - \nu\Delta T/3$ vs $T_m^0/fT(\Delta T)$, leading to Figure 10. All the different pressure experiments lead to a single curve which exhibits two linear parts characteristic of regimes II and III. The regime transition appears for $T_m^0/fT(\Delta T) = 2.204 \times 10^{-2}$ K^{-1}. After calculation for each pressure, this value corresponds to a constant regime transition undercooling $\Delta T = 54$ K. This result is very close to the result of Mezghani and Phillips for 200 MPa.[17] Indeed, they showed that the sign of birefringence of the spherulites changed in the vicinity of this undercooling value and they attributed this phenomenon to the II−III regime transition.[19]

The slopes of the modified Hoffman−Lauritzen diagram provide the values $K_g/T_m^0 = 681$ K in regime III and $K_g/T_m^0 = 340$ K in regime II, leading-to-a ratio of 2. The fact that the results merge now on the same pattern leads to conclude that the pressure affects the crystallization growth rate by its influence on the equilibrium melting temperature and on the diffusion. It must be pointed out that the slope values are approximately 20% higher than the previous results (Figure 8) meaning that the influence of the pressure on the diffusion is not negligible. However, one can argue if the choice of eq 18 and the fitted parameters are legitimate or not to describe this pressure effect. It must be recognized that, depending on the pressure and temperature fitting ranges, the variation of the obtained parameters could lead to slightly different results. Particularly, the different points could be somewhat more dispersed than in Figure 10 and the slopes slightly different also. Nevertheless, in that case, the slope ratio was not so close to 2 than for the present results. The choice of the values of α and β for eq 18 was then guided by the whole consistency of the results including the forthcoming features of the analysis where the slope values are required.

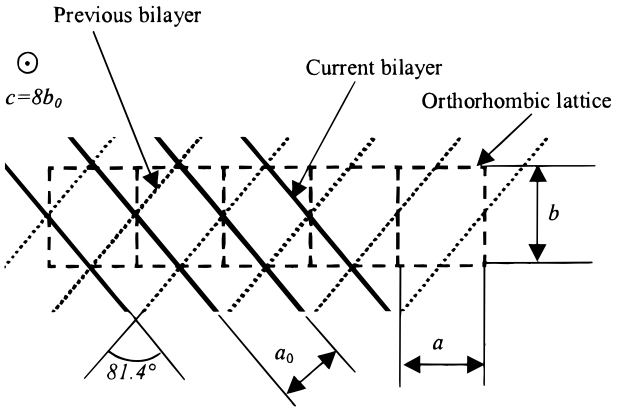

Figure 11. Scheme of the stems deposit on the growing γ crystal.

From either slopes of the straight lines in Figure 10, and using eq 6, the value of σ_e can be evaluated provided that the value of l_b/l_u, C_∞, a_0, and b_0 are known. The values of l_b/l_u and C_∞ for polypropylene can be obtained from the literature[24,50] ($l_b/l_u = 1.42$ and $C_\infty = 5.7$), but the evaluation of the width of the chain stem a_0 and the thickness of the molecular layer added b_0 have to be clarified because of the peculiarity of the γ crystalline phase. First, due to the nonparallel chain orientations, the most probable growth direction corresponds to the c-axis of the orthorhombic lattice.[51] Moreover, since there are 4 layers of 2 polymer chains in the c-axis direction, the layer thickness is

$$b_0 = \frac{c}{8} \tag{20}$$

Furthermore, as can be seen in Figure 11, the width of the chain stem is given by

$$a_0 = a\cos\left[\arctan\left(\frac{a}{b}\right)\right] \tag{21}$$

Thus, from the unit cell parameters given by Brückner et al.[38] ($a = 8.52$ Å, $b = 9.92$ Å and $c = 42.31$ Å), one obtains $a_0 = 6.46$ Å and $b_0 = 5.29$ Å. Then, using eq 6 (with $j = 4$ and $K_g/T_m^0 = 681$ K) the fold surface free

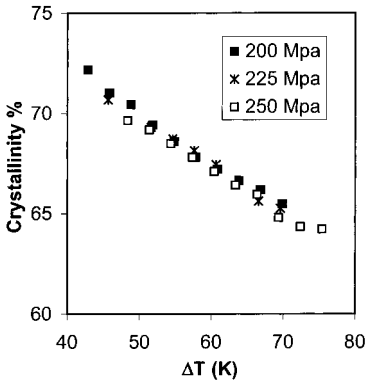

Figure 12. Crystallinity vs crystallization undercooling for three crystallization pressures.

energy is obtained: $\sigma_e = 55.2$ mJ·m^{-2} which is close to the value of 51.7 mJ·m^{-2} reported by Mezghani and Phillips.[16,18]

Furthermore, the lateral surface free energy σ can also be evaluated from eq 5. Using the value[16,18] of Δh_f of 144.8 J.g^{-1} and the crystal density $\rho_c = 0.938$ g·cm^{-3} given by Brückner et al.[38] one obtains $\sigma = 10.9$ mJ·m^{-2}.

Morphology. As concluded in the previous section, the pressure influences both surface nucleation and diffusion processes. Nevertheless, it has been shown that the pressure effect on the former process is fully taken into account by the equilibrium melting temperature change with the pressure. As a consequence, the final crystalline morphology of the samples should be only influenced by the crystallization undercooling, or, more rigorously, by the product $T\Delta T$, suggesting that the values of Δh_f, σ_e, and σ are practically independent of the pressure in the range investigated here.

The crystallinity obtained from density measurements of samples crystallized in different conditions of temperature and pressures is plotted against the crystallization undercooling in Figure 12. Again, the results are gathered in a single curve for the different pressures.

Moreover, from the long period L measured by SAXS the crystalline lamellar thickness l_c can be obtained by

$$l_c = LX_v \tag{22}$$

From a theoretical point of view, the crystalline lamellar thickness can be compared to the initial lamellar thickness l_g* defined by eq 3 if the isothermal thickening is neglected.[24] This comparison is displayed in Figure 13 showing a good agreement between measured and calculated values for two crystallization pressures. This result confirms independently the value of σ_e obtained from the kinetic analysis. It should be noticed that the additional length δ calculated by eq 4 accounts for 7−15% in the calculated values of l_g*. Furthermore, again by plotting the results vs the undercooling, the pressure effect is fully taken into account as can be seen in Figure 14.

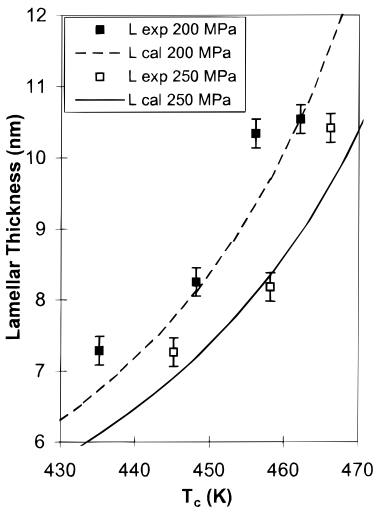

Figure 13. Measured and calculated lamellar thickness vs crystallization temperature for two crystallization pressures.

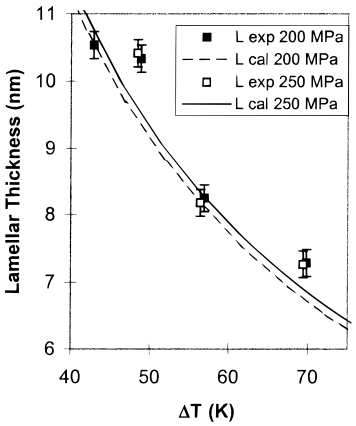

Figure 14. Measured and calculated lamellar thickness vs crystallization undercooling for two crystallization pressures.

Conclusions

The variation of the equilibrium melting temperature with the pressure was determined for the γ-form of iPP between 200 and 250 MPa by crystallization under pressure and subsequent melting. Then, following the Hoffman−Lauritzen theoretical frame, the crystallization regime analysis was carried out using the half-crystallization times. This analysis was refined to take into account the effects of the pressure. First, it was shown that the number of heterogeneous nuclei depends on the crystallization undercooling and the corresponding correction was introduced. Moreover, we propose a modification of the classical Hoffman−Lauritzen diagram leading to the plot of the results against $T_m^0/fT(\Delta T)$ in order to completely take into account the effects of the pressure on the growth rate. Furthermore, based on literature results, a correction of the diffusion term was introduced. The final modified plot appears correctly normalized respectively to the pressure, revealing a II−III regime transition for an undercooling of 53.7 K with a slope ratio of 2 as theoretically expected. The fold and lateral surface free energies were calculated ($\sigma_e = 55.2$ mJ·m^{-2} and $\sigma = 10.9$ mJ·m^{-2}). Besides, based on crystallinity and lamellar thickness measurements, it was shown that the final morphology of the samples only depends on the crystallization undercooling. Moreover, the measured lamellar thickness are in good agreement with theoretical calculations, consistent with the deduced surface free energy values.

Acknowledgment. The authors would like to thank the ATOCHEM Co. for its financial support, material supply, and molecular characterization.

References and Notes

(1) Natta, G.; Corradini, P. *Nuovo Cimento Suppl.* **1960**, *15*, 40.
(2) Turner-Jones, A.; Aizlewood, J. M.; Beckett, D. R. *Makromol. Chem.* **1964**, *75*, 134.
(3) Keith, H. D.; Padden, F. J., Jr.; Walter, N. M.; Wickoff, H. W. *J. Appl. Phys.* **1959**, *30*, 1485.
(4) Meille, S. V.; Ferro, D. R.; Brückner, S.; Lovinger, A. J.; Padden, F. J. *Macromolecules* **1994**, *27*, 2615
(5) Lotz, B.; Kopp, S.; Dorset, D. *C. R. Acad. Sci. Paris, Ser. Iib* **1994**, *319*, 187.
(6) Brückner, S.; Meille, S. V. *Nature* **1989**, *340*, 455.
(7) Meille, S. V.; Brückner, S.; Porzio, W. *Macromolecules* **1990**, *23*, 4114−4121.
(8) Lotz, B.; Graff, S.; Straupé, C.; Wittmann, J. C. *Polymer* **1991**, *32*, 2902−2910.
(9) Lotz, B.; Wittmann, J. C.; Lovinger, A. J. *Polymer* **1996**, *37*, 4979−4992.
(10) Morrow, D. R.; Newman, B. A. *J. Appl. Phys.* **1968**, *39*, 4944.
(11) Turner-Jones, A. *Polymer* **1971**, *12*, 487.
(12) Mezghani, K.; Phillips, P. J. *Polymer* **1995**, *36*, 2407−2411.
(13) Sauer, J. A.; Pae, K. D. *J. Appl. Phys.* **1968**, *39*, 4959.
(14) Nakafuku, C. *Polymer* **1981**, *22*, 1673.
(15) Campbell, R. A.; Phillips, P. J.; Lin, J. S.,*Polymer* **1993**, *34*, 4809−4816.
(16) Mezghani, K.; Phillips, P. J. *SPE ANTEC '95* **1995**, 1492−1496.
(17) Mezghani, K.; Phillips, P. J. *Polymer* **1997**, *38*, 5725−5733.
(18) Mezghani, K.; Phillips, P. J. *Polymer* **1998**, *39*, 3735−3744.
(19) Phillips, P. J. Private communication.
(20) Kishore, K.; Vasanthakumari, R. *High Temperatures−High Pressures*, **1984**, *16*, 241−268.
(21) He, J.; Zoller, P. *J. Polym. Sci., Part B: Polym. Phys.* **1994**, *32*, 1049−1067.
(22) Lauritzen, J. I., Jr.; Hoffman, J. D. *J. Appl. Phys.* **1973**, *44*, 4340−4352.
(23) Hoffman, J. D.; Davis, G. T.; Lauritzen, J. I., Jr. In *Treatise on Solid State Chemistry*; Hannay, N. B., Ed.; Plenum Press: New York, 1976; Vol. 3, Chapter 7.
(24) Hoffman, J. D.; Miller, R. L. *Polymer* **1997**, *38*, 3151−3212.
(25) Williams, M. L.; Landel, R. F.; Ferry, J. D. *J. Am. Chem. Soc.* **1955**, *77*, 3701.
(26) Lee, W. A.; Knight, G. J. *Br. Polym. J.* **1970**, *2*, 73−80.
(27) Clark, E. J.; Hoffman, J. D. *Macromolecules* **1984**, *17*, 878−885.
(28) Monasse, B.; Haudin, J. M. *Colloid Polym. Sci.* **1988**, *266*, 679−687.
(29) Janimak, J. J.; Cheng, S. Z. D.; Giusti, P. A.; Hsieh, E. T. *Macromolecules* **1991**, *24*, 2253−2260.
(30) Hoffman, J. D. *Polymer* **1982**, *23*, 656−670.
(31) Perez, J.; Cavaillé, J. Y.; David, L. *J. Mol. Struct.* **1999**, *479*, 183−194.
(32) Santangelo, P. G.; Ngai, K. L.; Roland, C. M. *Macromolecules* **1996**, *29*, 3651−3653.
(33) Hoffman, J. D. *Polymer* **1992**, *33*, 2643−2644.
(34) Flory, P. J. In *Statistical Mechanics of Chain Molecules*; Wiley-Interscience: New York, 1969; Chapter 1.
(35) Thomann, R.; Wang, C.; Kressler, J.; Mülhaupt, R. *Macromolecules* **1996**, *29*, 8425−8434.
(36) Vigier, G.; Tatibouet, J.; Benatmane, A.; Vassoile, R. *Colloid Polym. Sci.* **1992**, *270*, 1182−1187.
(37) Santa Cruz, C.; Stribeck, N.; Zachmann, H. G.; Balta Calleja, F. J. *Macromolecules* **1991**, *24*, 5980−5990.
(38) Brückner, S.; Phillips, P. J.; Mezghani, K.; Meille, S. V. *Macromol. Rapid Commun.* **1997**, *18*, 1−7.
(39) Miller, R. L. In *Polymer Handbook*; Brandrup, J., Immergt, E. H., Eds.; J. Wiley & Sons-Interscience Publishers: New York, 1966, Chapter III.
(40) Hoffman, J. D.; Weeks, J. J. *J. Res. Natl. Bur. Stand.* **1962**, *66A*, 13−28.
(41) Billon, N.; Escleine, J. M.; Haudin, J. M. *Colloid. Polym. Sci.* **1989**, *267*, 668−680.
(42) Varga, J. *Angew. Makromol. Chem.* **1983**, *112*, 161.
(43) Binsbergen, F. L. *J. Polym. Sci., Polym. Symp.* **1977**, *59*, 11−29.
(44) Wunderlich, B. *Macromolecular Physics*; Academic Press: New York, 1976; Vol. 2 (Crystal Nucleation, Growth, Annealing), Chapter 5.
(45) Rybnikar, F. *J. Appl. Polym. Sci.*, **1982**, *27*, 1479−1486.
(46) Doi, M.; Edwards, S. F. In *The Theory of Polymer Dynamics*; Clarendon Press: Oxford, England, 1986, Chapter 7.
(47) Cogsweel, F. N.; McGowan, J. C. *Br. Polym. J.* **1972**, *4*, 183−198.
(48) Zoller, P. *J. Polym. Sci., Part B: Polym. Phys.* **1982**, *20*, 1453−1464.
(49) Kadijk, S. E.; Van Den Brule, B. H. A. A. *Polym. Eng. Sci.* **1994**, *34*, 1535−1546.
(50) Hoffman, J. D.; Miller, R. L.; Marand, H.; Roitman, D. B. *Macromolecules* **1992**, *25*, 2221−2229.
(51) Meille, S. V.; Ferro, D. R.; Brückner, S. *Macromol. Symp* **1995**, *89*, 499−511.

MA991813E